Presented at the IEEE 1978 Nuclear
Science Symposium, Washington D.C.,
October 18-20, 1978

LBL-8327

EXPERIMENTAL STUDY OF THE SIGNALS FROM A SEGMENTED CATHODE DRIFT CHAMBER

D. L. Fancher and A. C. Schaffer

October 1978

Prepared for the U. S. Department of Energy
under Contract W-7405-ENG-48

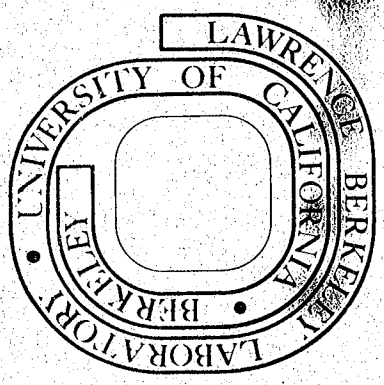

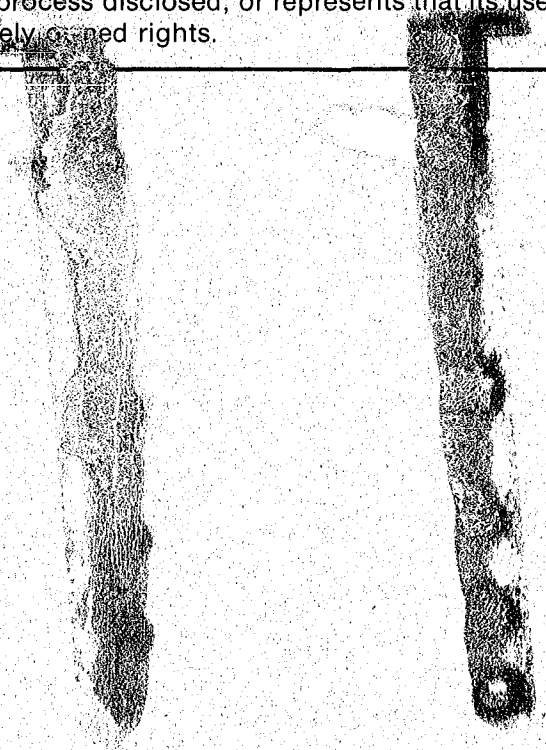

EXPERIMENTAL STUDY OF THE SIGNALS FROM A SEGMENTED CATHODE DRIFT CHAMBER*

D. L. Fancher† and A. C. Schaffer§

Abstract

A test drift chamber has been constructed with a segmented cathode for measuring the second coordinate. A corona discharge source has also been constructed to measure the response of the cathode segments. Various size segments were studied and the position resolution and pulse height distributions measured.

I. Introduction

A proportional drift chamber has been designed to study the properties of signals induced on various configurations of segmented cathodes, or "pads". The specific goals of the study were to measure the dependence on the size and shape of various pad geometries, and on the distance of the pads from the position of the proportional avalanche. From this information an optimum configuration of pads can be determined for the Time Projection Chamber[1] (TPC) now being constructed at the Lawrence Berkeley Laboratory (LBL) for installation at the Positron-Electron colliding beam accelerator (PEP) at Stanford. In addition, the position resolution and pulse height distributions (response functions) for the various pad types were determined.

In the TPC, ionization electrons left by a passing charged particle drift under the influence of parallel electric and magnetic fields onto a set of proportional wires. The proportional wires sample energy loss for particle identification purposes, and also define the coordinate Y perpendicular to the sense wires. (X, Y, and Z are defined in Fig. 1a.) Sets of induction pads[2] under some of the wires are used to measure the coordinate along the sense wire, X. Measuring the drift time of the ionization electrons (the time between the particle crossing and the appearance of the signals on the wires and pads) gives a measure of the coordinate in the drift direction, Z.

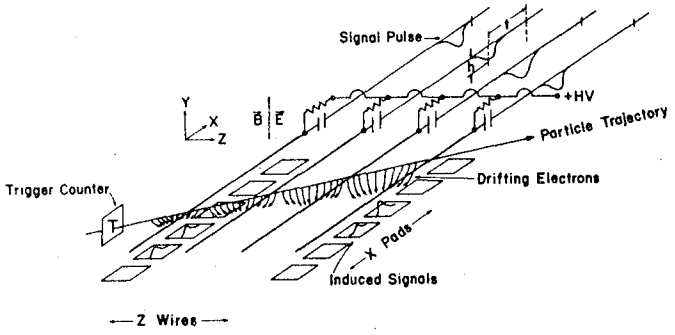

Bevatron TPC - Principle of Operation

XBL 7612-11286

Fig. 1a. TPC Principle of Operation. Drifting electrons are captured by proportional wires. Induction pads measure the coordinate X. The wires measure the coordinate Y as well as providing energy loss information. The drift time t measures the coordinate Z.

This time measurement is done using analog shift registers (charge coupled devices - CCD's) to store the pulse height information from the wires and cathode pads as a function of time. A CCD prototype system has been built and extensively tested in a particle beam and is the subject of another paper submitted to this conference.

In order to determine the optimum pad configuration for the TPC, a small chamber with four sizes of pads was constructed and tested. The goal of the study was to determine an optimum pad size that used the fewest number of channels while still maintaining an adequate resolution in X. The desired spatial resolution for the TPC was 200 microns. The chamber is described in the next section. An electron gun was also constructed to define a well-collimated pulsed source of electrons for the tests and is described, along with the results of the data analysis, in subsequent sections.

II. The Chamber

The pad chamber, see Figs. 1b, 2, 3, and 4, consists of two planes of wires and one plane of pads. The geometry closely resembles the design configuration in the final TPC.

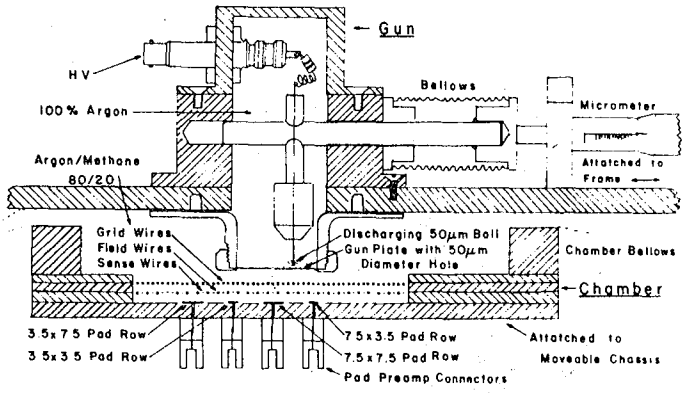

Cathode Pad Chamber and Discharge Source

FIG. 1b

XBL 786-10434

Fig. 1b. Cut away drawing of the pad prototype chamber and the corona discharge source (gun).

*Work has been supported by the High Energy Physics Division of the U.S. Department of Energy.
†Lawrence Berkeley Laboratory, University of California, Berkeley, CA 94720.
§Present address: Department of Physics, Columbia University, New York, NY 10027.

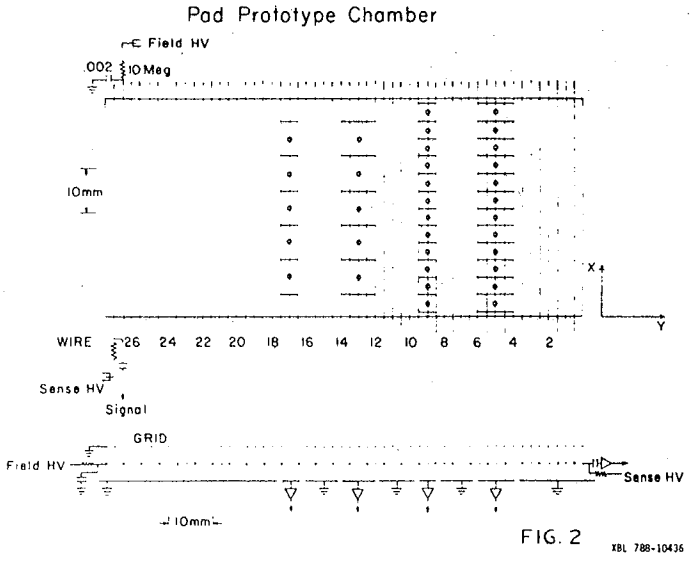

Fig. 2. Detailed layout of the pad prototype system.

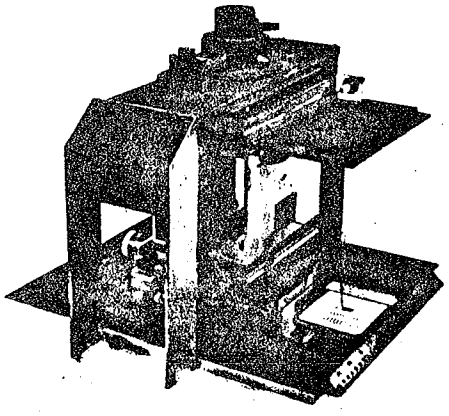

Fig. 3. Photograph of the pad prototype chamber with the corona discharge gun and the mechanism for scanning the chamber with the gun.

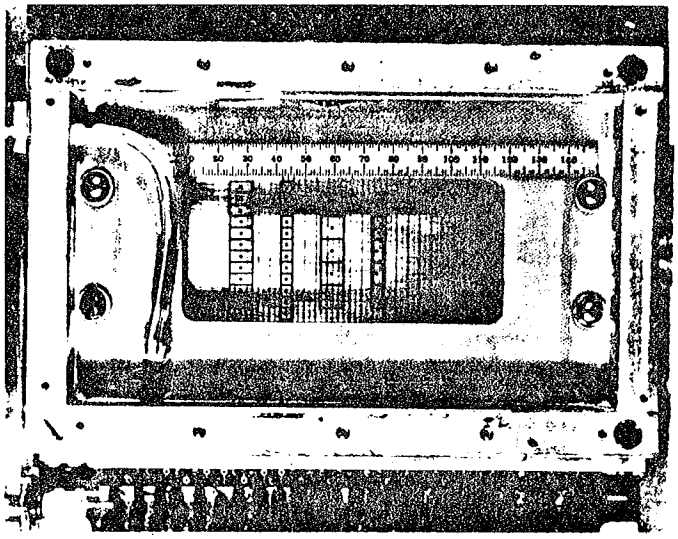

Fig. 4. Photograph looking down on the pad chamber illustrating the four pad types and the wire planes.

The operating and physical characteristics of this three-plane chamber are given in Table I. The uppermost plane, or "grid" plane, consists of grounded wires with 2mm spacing, which isolates the drift region from the proportional region. The next lower layer (refer to Fig. 2) contains alternating "field" and "sense" wires, each wire lying directly below a grid wire. The field and sense wire spacing is 2mm. Each field wire is AC coupled to ground and each sense wire is AC coupled to a low-noise charge-sensitive FET preamplifier. The sense and field wire voltages could be independently set via external bus lines coupled to each wire through a ten megohm resistor. The third plane is a gold-coated copper-plated ground plane onto which four rows of induction pads are etched. Each pad row is parallel to, and centered under, a sense wire and contains a different size of rectangular pad. Each pad is directly coupled to a low-noise charge-sensitive FET preamplifier.

TABLE I. Properties of the Pad Chamber

Wires:

Type	Material	Diameter
Grid and Field	Stainless Steel	75 μm
Sense	Gold-coated Tungsten	20 μm

Number of Grid Wires:	54
Number of Field Wires:	27
Number of Sense Wires:	27
Wire Spacing:	2 mm
Plane Spacing:	4 mm
Gas:	1 atm, 80% Ar - 20% CH_4

(Table I continued next page)

(Table I. Continued)

Pads:	
Row 1	7.5 mm × 3.5 mm*
Row 2	7.5 mm × 7.5 mm
Row 3	3.5 mm × 3.5 mm
Row 4	3.5 mm × 7.5 mm
Material:	gold-plated copper
Gap between adjacent pads:	0.5 mm
Space between pad rows:	16 mm

*First dimension is always in the direction parallel to the wires.

An Fe^{55} x-ray source was located at the edge of the chamber away from the pad rows. This source served to monitor the gas gain stability of the chamber. The chamber was attached to a moveable x-y stage, shown in Fig. 3. The corona discharge gun, to be described in the next section, was mounted in a fixed position above the chamber. The chamber was attached to the gun via a flexible bellows and the chamber could be moved under the gun so as to scan the electron source parallel to and perpendicular to the wires. The gun could easily be moved anywhere over the chamber.

III. The Corona Discharge Source (Electron Gun)

A corona discharge source (electron gun) has been constructed to provide a well-collimated source of thermal electrons with which the position response of the chamber could be measured. The gun, shown in Fig. 1b, is a pulse discharge relaxation oscillator wherein the capacitor is formed by a ball-tipped wire above a thin circular plate. The electrons pass through a 50 μm hole in the plate. A negative potential was placed on the plate so that electrons, once through the hole, drifted towards the chamber.

The ball was melted onto the end of a platinum wire. The ball could be moved, via a micrometer, in order to adjust the spacing between the ball and the plate.

The gun chamber was gas tight except for the 50 μm hole in the plate. The gun chamber was flushed continuously with a high flow rate of pure argon gas at a slightly higher pressure than the pad chamber in order to keep methane from the pad chamber out of the gun chamber. It was found that the methane would form deposits on the ball surface when the gun was discharged for periods of time.

The gun plate was kept at -75v; this established a drift field of 150 V/cm or an E/p of 0.2 V/cm/torr. This corresponds to the E/p expected to be used in the TPC.

The effective width of the source at the grid plane is essentially determined by diffusion in the electron bunch emitted from the plate hole. For the operating conditions, with no magnetic field, and with a 5 mm drift region, the width from diffusion is σ_D = 350 μm.[1] The pulse width of the gun was considerably less than the shaping time of the amplifiers we used.

After considerable experimentation, the gun was operated successfully and with good stability over long periods of time. After a warmup period of several hours, the gun ran at a frequency of 7 to 12 kHz. The measured RMS of the pulse height distribution on a wire was in the range of 6 to 10 percent. (See Fig. 5, and note the suppressed zero.) There was a slow drift in this pulse height with time which was easily correctable. The stability of the gun was more than adequate for the data scans.

Table II summarizes the properties of the gun.

TABLE II. Properties of the Corona Discharge Source

Circular Plate:	
Material:	50 μm gold foil
Diameter:	20 mm
Hole diameter:	50 μm
Distance from grid plane:	5 mm
Discharging Wire:	
Material:	Platinum
Diameter:	25 μm
Ball diameter:	50 μm
Distance of ball from plate:	1 mm
Series resistance:	1100 megohm

IV. Data Taking

The data consisted of scans taken by moving the chamber in prescribed steps under the gun. Scans were taken along each pad row in directions both parallel to and perpendicular to the wire direction. Scans were taken along the sense wires located above the centers of each pad row. More scans were taken along other sense wires located adjacent to these sense wires. Scans were taken perpendicular to the sense wires along two lines, one centered above a pad, and the other centered above the boundary between two pads.

Data were taken by moving the chamber in increments of 0.5 mm or 1.0 mm. At each point in the scan, the pulse height spectra on all relevant sense wires and pads were measured. Figure 5 shows a typical wire pulse height spectrum and Fig. 6 shows the spectra from three adjacent pads when the gun was located between two of the pads.

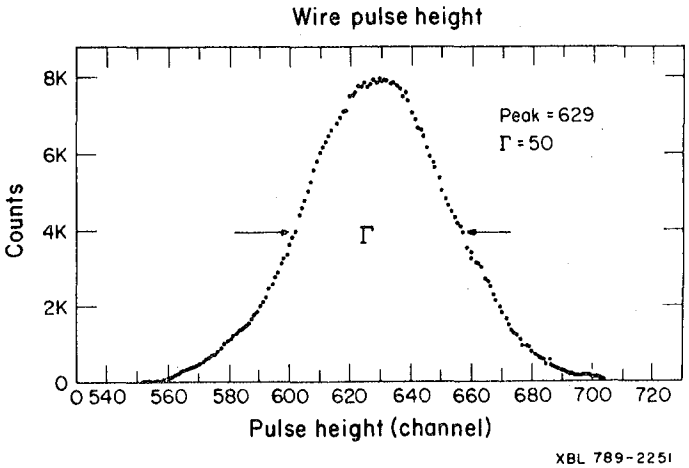

Fig. 5. PHA spectra on a sense wire from gun.

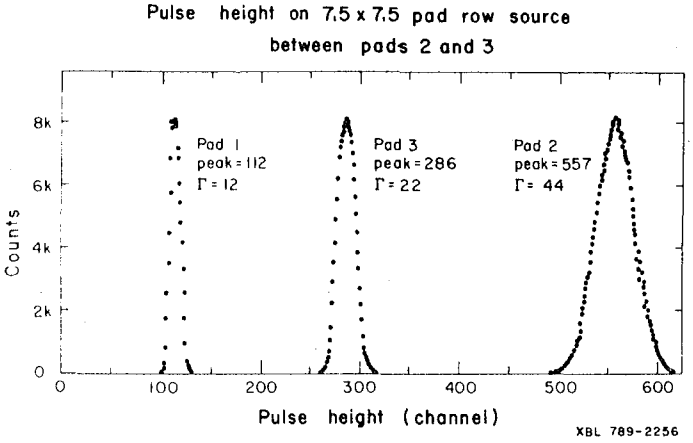

Fig. 6. PHA spectra from three adjacent pads from gun located between two of the pads.

At the end of each scan, the beginning points were re-measured to determine the drift in intensity of the gun signal during the scan. The raw data were corrected for any gun drift. Data from all the wires and pads were corrected for variations in preamplifier and amplifier gains and the PHA pedestal was subtracted. The pad peaks were normalized to the wire pulse height to correct for gain and gun amplitude variations along the wire. The PHA linearity was measured, and found to be good enough so that no linearity corrections were deemed necessary.

The spectrum from the Fe^{55} source, located above a particular sense wire, was measured periodically to keep track of any variations in gas gain. A typical Fe^{55} spectrum is shown in Fig. 7. The main peak (5.9 keV) and the escape peak (3.0 keV) are clearly seen.

V. Data Analysis

The corrected data from the scans described in the previous section were analyzed to learn the properties of each of the pad configurations. The description of the analysis will be broken into four parts.

First, scans along the pad rows were fit to determine the pad response functions for each pad geometry. This parameterizes the response of each pad as a function of the position where the ionization occurs with respect to the pad. From these response functions we have calculated the expected "best possible" position resolution obtainable from each pad type. This position resolution assumes that only noise contributes to the measured position error.

Next, we discuss the scans done along wires adjacent to the central wire above a pad row and the scans done perpendicular to the wires. Also described are our results on crosstalk between adjacent wires, noise, and gain measurements.

Then the pad data are used to represent what would be actually measured for a real track in the TPC and the actual pad position resolution in the TPC is computed as a function of where the "track" crosses the pad row. Also, various algorithms for determining the "track" position are compared.

Finally, the results of a test where a spacer was inserted between the sense plane and the ground plane to increase the distance between the sense wires and the pads from 4 mm to 5.5 mm are described.

The data were fit first to a simple solid-angle model. That is, the pulse height measured by the pad was assumed to be proportional to the solid angle subtended by the pad with respect to the point where the avalanche occurred. The solid-angle model appears to fall off more slowly than the data as the source moves away from the center of the pad.

On the other hand, a Gaussian function seems to fit the data well, as shown by Fig. 8. However, when the best Gaussian fit is subtracted from the data, a residual with a definite shape is left. The residual is plotted in Fig. 9.

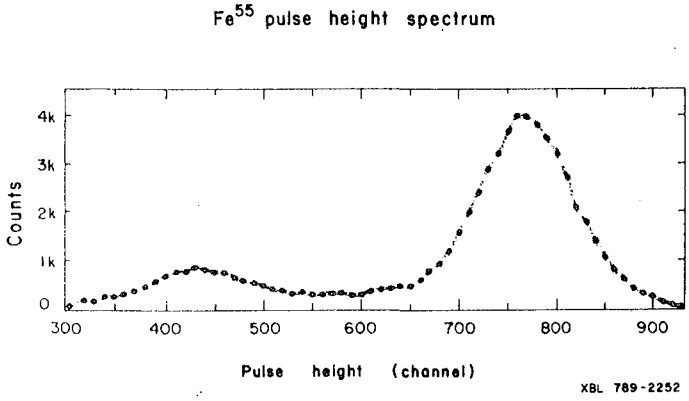

Fig. 7. Typical PHA spectra of an Fe^{55} source located above a sense wire.

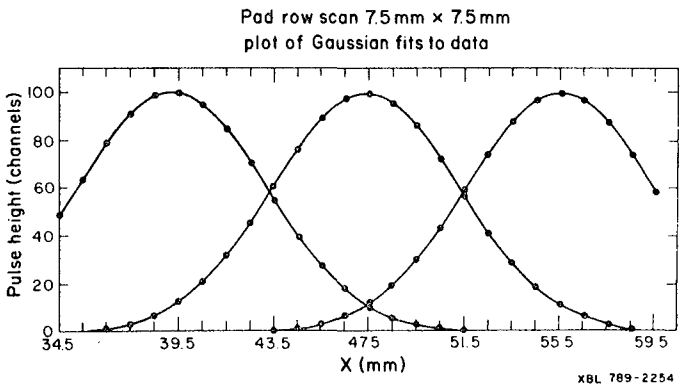

Fig. 8. Scan across a 7.5 mm x 7.5 mm pad row.

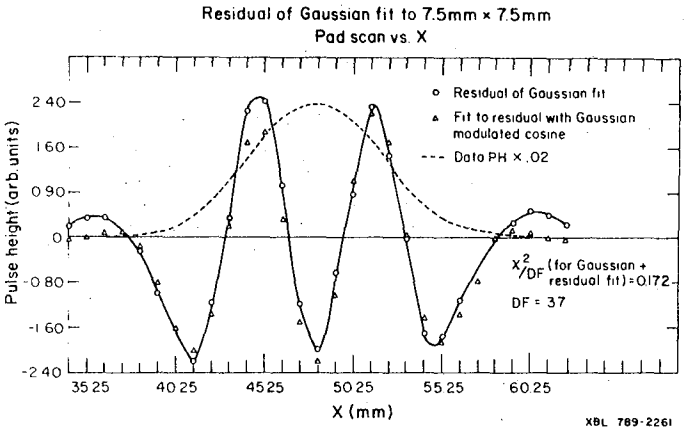

Fig. 9. Residual of Gaussian fit to data scan.

The residual is about two percent of the main signal and can be fit by a damped cosine function. The addition of such a correction term reduces the chi-square per degree of freedom of the fit by a factor of sixteen. A summary of the fits for the main wire scan, along with fits for scans along the wire adjacent to the main wire scan are given in Table III.

TABLE III. Pad Scan Fit Results

7.5 mm × 7.5 mm Pads

Fit 1 - Gaussian Fit Only					
Scan	σ	Peak	$\bar{x}$(mm)	x^2/DF	DF
Main Wire					
Pad 2	3.64	1.102	40.11	2.64	17
Pad 3	3.62	1.139	48.15	2.46	23
Pad 4	3.61	1.107	56.21	2.65	23
1st Adjacent (Inside)					
Pad 2	3.81	1.433	40.09	1.66	18
Pad 3	3.79	1.473	48.13	1.08	27
Pad 4	3.79	1.447	56.18	1.23	24
2nd Adjacent (Outside)					
Pad 2	3.80	1.351	40.00	1.76	17
Pad 3	3.80	1.393	48.11	1.10	25
Pad 4	3.81	1.364	56.14	1.08	25

$$\text{fit} = \text{peak} \cdot e^{\frac{-(x-\bar{x})^2}{2\sigma^2}}$$

(Table III continued next page)

Table III. (Continued)

Fit 2 - Gaussian + Residual Fit							
Scan	σ	Peak	$\bar{x}$(mm)	A	N	t(mm)	x^2/DF
Main Wire							
Pad 2	3.61	1.107	40.12	0.023	0.92	5.0	0.21
Pad 3	3.60	1.144	48.15	0.024	0.89	5.5	0.16
Pad 4	5.59	1.112	56.21	0.024	0.90	5.5	0.12
1st Adjacent (Inside)							
Pad 2	3.79	1.436	40.09	0.016	0.93	5.7	0.45
Pad 3	3.79	1.475	48.13	0.012	0.94	6.2	0.40
Pad 4	3.78	1.449	56.18	0.014	0.89	7.2	0.18
1st Adjacent (Outside)							
Pad 2	3.78	1.357	40.10	0.020	0.90	4.3	0.24
Pad 3	3.80	1.391	48.11	0.015	0.85	7.0	0.18
Pad 4	3.80	1.366	56.14	0.014	0.89	6.8	0.13

$$\text{fit} = \text{peak} \cdot e^{\frac{-(x-\bar{x})^2}{2\sigma^2}} - A \cdot \text{peak} \cdot e^{\frac{-(x-\bar{x})^2}{2t^2}} \cos\left(N(x-\bar{x})\right)$$

Figures 10, 11, and 12 show the data scans along the main sense wires for the other pad rows.

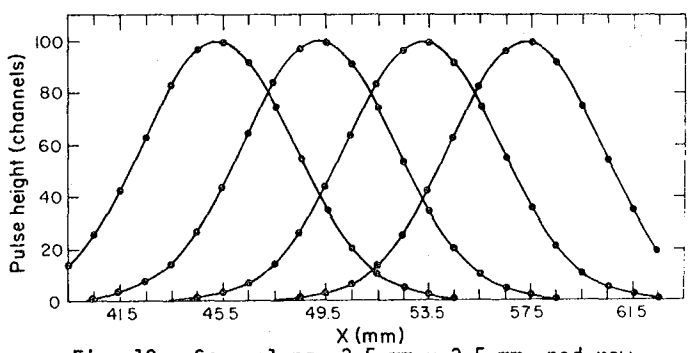

Fig. 10. Scan along 3.5 mm × 3.5 mm pad row.

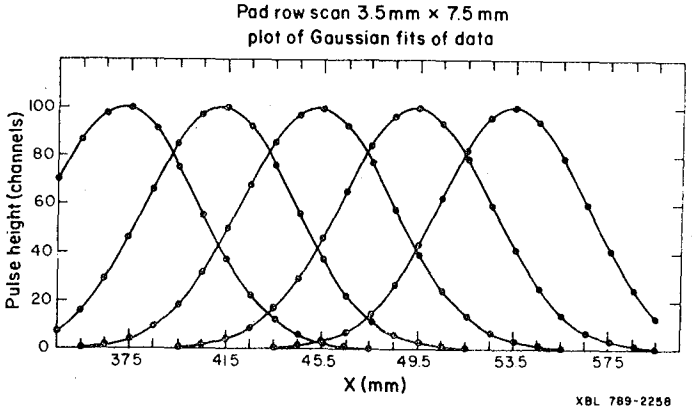

Fig. 11. Scan along 3.5 × 7.5 mm pad row.

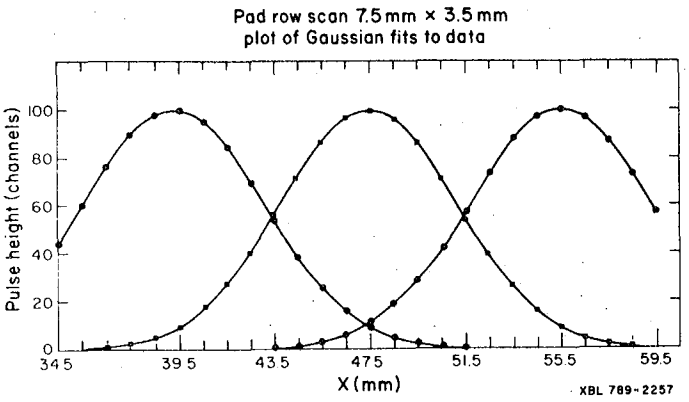

Fig. 12. Scan along 7.5 mm x 3.5 mm pad row.

Figure 13 shows the pad respose functions for each of the pad types as well as for the 7.5 mm x 7.5 mm pads with the spacer in. The relative sizes and widths are clearly shown.

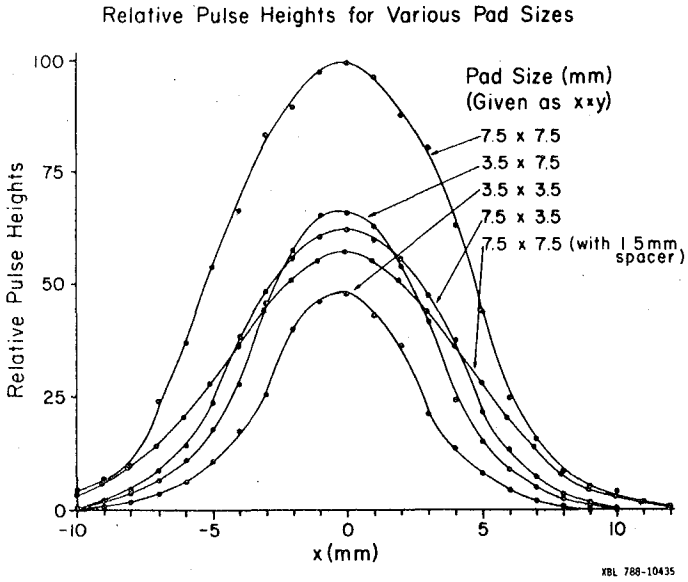

Fig. 13. Pad response functions for various pad types.

Table IV summarizes the differences between the pad types.

TABLE IV. Relative Pad Signals
(normalized to wire pulse height = 1.0)

Pad Size (mm × mm)	Pad Pulse Height measured	solid angle model	normalized to 7.5 × 7.5 pad
7.5 × 7.5	0.195	0.310	1.0
7.5 × 3.5	0.103	0.177	0.65
3.5 × 7.5	0.102	0.177	0.64
3.5 × 3.5	0.064	0.103	0.40
7.5 × 7.5 (with spacer)	0.090	0.206	0.56

Scans were also taken along lines off to the side of the pad rows. Figure 14 compares a scan taken just inside the first adjacent wire with the scan taken over the main wire.

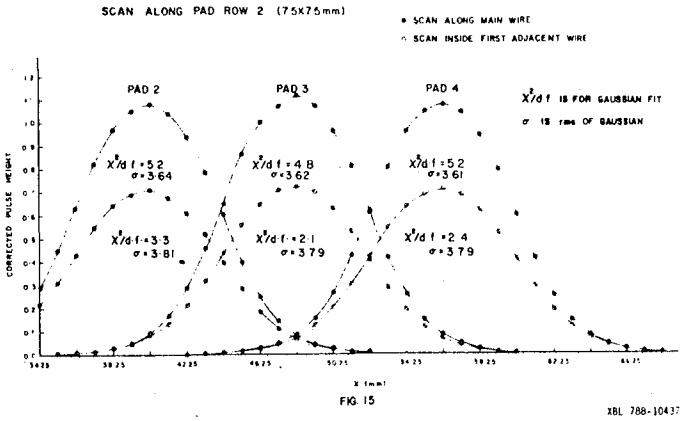

Fig. 14. Scan along 7.5 mm × 7.5 mm pad plus adjacent wire scan and with Gaussian fits.

The Gaussian model was found to fit these adjacent wire scans fairly well, but the width of the distribution was found to increase with increasing distance from the main sense wire. Figure 15 shows the results of a scan perpendicular to the wires.

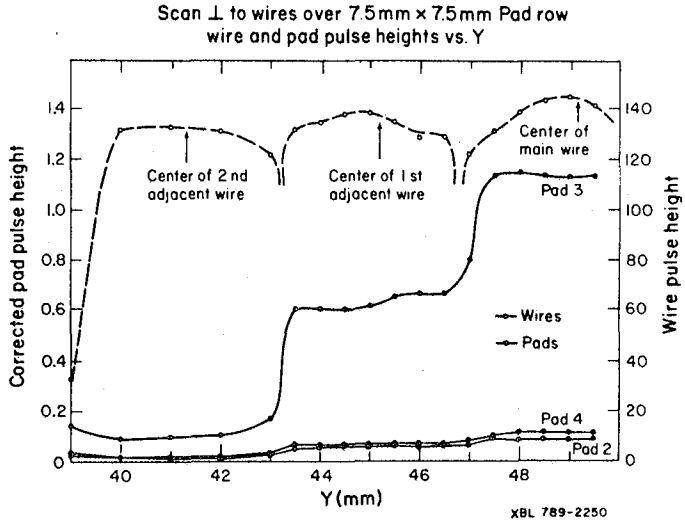

Fig. 15. Pad and wire pulse heights from scan perpendicular to the wires from center of 7.5 mm × 7.5 mm pad number 3.

From these measurements we can deduce the relative contributions to the pad pulse height from each of the sense wires. For example, for the 7.5 mm × 7.5 mm pads, the total pad pulse height is made up of a 42% contribution from the main sense wire, 25% from each of the adjacent sense wires, and 4% from each of the second-most adjacent sense wires. Other sense wires contribute negligibly to the pad pulse height. Table V summarizes the contributions to the total pad pulse height from the adjacent wires.

TABLE V. Signals on Pads Due to Adjacent Wires

Pad Type	Source Placement	Pad Signal Contribution: 1st adj.wire / main wire	Pad Signal Contribution: 2nd adj.wire / main wire
7.5mm × 7.5mm	Between Pads	0.616	0.117
	Over Pad	0.596	0.118
3.5mm × 7.5mm	Between Pads	0.614	0.116
	Over Pad	0.616	0.112
7.5mm × 3.5mm	Between Pads	0.411	0.066
	Over Pad	0.395	0.060
3.5mm × 3.5mm	Between Pads	0.469	0.074
	Over Pad	0.487	0.064

The measured RMS noise on the chamber was 0.64% for the 7.5 mm × 7.5 mm pads and 0.3% for the wires. Measurement errors were also of this size. The crosstalk between wires was also measured. The crosstalk was measured on 16 wires and the results averaged. The pulse height on the first adjacent wire was 4.5% of the main wire pulse height. The pulse height on the second adjacent wire was 1.4% of the main wire pulse height. This figure is not corrected for the crosstalk between the first adjacent wire and the second adjacent wire.

The wire gain of the chamber was measured as a function of chamber high voltage and the results are summarized in Table VI. The preamp feedback capacitor was 1.0 pf.

TABLE VI. Chamber Gain

Sense Hv (volts)	Fe^{55} Peak Preamp Signal (mv)	Wire Gain
1150	8.1	230
1200	13.5	383
1250	21.6	614
1300	33.78	960

We now turn our attention to the estimation of position measurement errors based on the measured pad response functions.

If we assume that the pad response functions are Gaussian, and that the only error in the measurements of the pad pulse heights is from noise (0.64% mentioned previously) then we can compute the mean position error σ_x (the error in measurement of the coordinate X of Fig. 1a) for each pad row as a function of the distance X along the pad row. The variation in σ_x is shown in Fig. 16.

Theoretical mean position error σ_x for each pad type for 1.28% pulse height measurement error

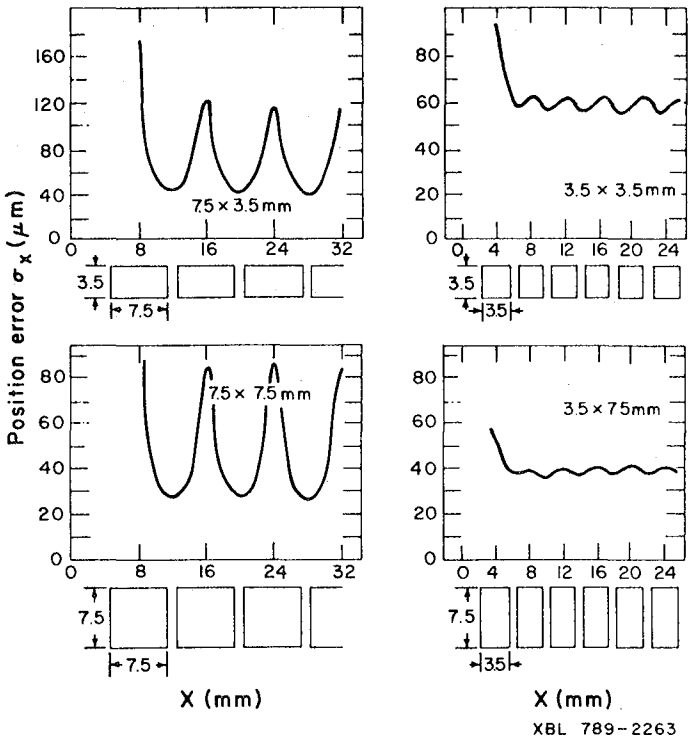

Fig. 16. Best possible position error σ_x for each pad type.

The pulse height variation of the rows is included in this calculation. The 0.64% noise is relative to the pulse height at the center of a 7.5 mm × 7.5 mm pad. Smaller pads have a smaller signal and hence larger relative noise, even though they sample the distribution with a smaller spacing. Table VII shows the relative values of noise for each pad row. The variation in σ_x with X (σ_x is largest at the center of a pad) is due to the fact that, at the center of a pad, the contribution from the neighboring pads is a minimum and the relative noise is the largest.

TABLE VII. Relative Pad Noise

Pad Row (mm × mm)	Normalized Peak Pulse Height	σ_{noise} (mv)
7.5 × 7.5	1.0	6.4/1.00 = 6.4
7.5 × 3.5	0.65	6.4/0.65 = 9.8
3.5 × 7.5	0.64	6.4/0.64 = 10.0
3.5 × 3.5	0.40	6.4/0.40 = 16.0
7.5 × 7.5 (with spacer)	0.56	6.4/0.56 = 11.4

Of course, the actual measurement error will be subject to additional sources of error, such as diffusion, multiple scattering and pad location uncertainties, to name a few. To attempt to estimate actual position measurement errors, we computed the difference between the actual gun position and the gun position computed from the pad data. This

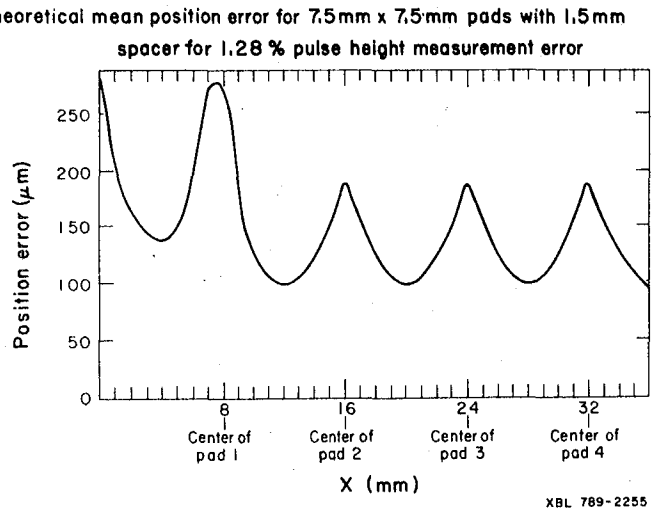

Fig. 21. Theoretical position error for 7.5 mm × 7.5 mm pad row with spacer.

In conclusion, the pad chamber has provided considerable useful information concerning pad response functions and pad measurement errors for pads suitable for use in the TPC. Measurement errors, even for the largest pads considered, are better than necessary for the TPC. A Gaussian response function was found to fit the data fairly well. It should be mentioned, that while such a function has no apparent theoretical basis, the actual pad response functions are being calculated; results should be available in the near future. Also, a prototype TPC has been installed in a 1.8 GeV/c proton beam at the Bevalac and the mean pad position error for 7.5 mm × 7.5 mm pads was measured to be 100 ± 3 μm.[3]

References

1. Proposal for a PEP Facility Based on the Time Projection Chamber, PEP-4, PUB-5012 (December 1976).
2. Induction pad readout is discussed in: G. Charpak et al., CERN 73-11, 1973; G. Charpak et al., NIM 113 (1973) 381; G. Charpak, IEEE Transactions of Nuclear Science, NS-21, No. 1, p. 38, 1974; A/P. Jeavons et al., IEEE Transactions of Nuclear Science, NS-23, No. 1, p. 259, 1974.
3. D. Fancher et al., Performance of a Time-Projection Chamber, April 14, 1978, to be submitted to Nuclear Instruments and Methods.

This report was done with support from the Department of Energy. Any conclusions or opinions expressed in this report represent solely those of the author(s) and not necessarily those of The Regents of the University of California, the Lawrence Berkeley Laboratory or the Department of Energy.

TECHNICAL INFORMATION DEPARTMENT
LAWRENCE BERKELEY LABORATORY
UNIVERSITY OF CALIFORNIA
BERKELEY, CALIFORNIA 94720